Theoretical study of the electronic and magnetic structures of the Heusler alloys $Co_2Cr_{1-x}Fe_xAl$

V. N. Antonov,[1] H. A. Dürr,[2] Yu. Kucherenko,[1] L. V. Bekenov,[1] and A. N. Yaresko[3]
[1]*Institute of Metal Physics, National Academy of Sciences of Ukraine, UA-03142 Kiev, Ukraine*
[2]*BESSY GmbH, D-12489 Berlin, Germany*
[3]*Max Planck Institute for the Physics of Complex Systems, D-01187 Dresden, Germany*
(Received 16 December 2004; revised manuscript received 20 May 2005; published 26 August 2005)

The electronic structure, x-ray absorption (XAS), x-ray magnetic circular dichroism (XMCD), and magneto-optical spectra of the doped Heusler alloys $Co_2Cr_{1-x}Fe_xAl$ ($x=0$, 0.125, 0.25, 0.375, 0.5, 0.625, 0.75, and 1) were investigated theoretically from first principles, using the fully relativistic Dirac linear-muffin-tin-orbital band structure method. It was shown that the concentration and arrangement of Fe atoms in the lattice play the leading role in the formation of the magnetic properties of the compounds, determining to a considerable extent the magnetic states of Co and Cr atoms. The spin polarization of electron states at the Fermi energy is quite high (about 95%) for the compositions between $x=0$ and $x=0.4$, owing to the presence of high peaks of majority-spin Cr and Co d density of states at the Fermi energy. Further increasing of Fe content leads to the abrupt decreasing of the spin polarization of carriers. The band structure calculations in the LSDA approximation reproduce quite well the shape of the XAS and XMCD spectra at the Co, Fe, and Cr $L_{2,3}$ edges. The energy dependence of the matrix elements affects strongly the values of both the spin and the orbital magnetic moments derived from the calculated XAS and XMCD spectra using the sum rules. Our calculations show that the magneto-optical measurements are sensitive to changes in the structure of compounds (doping, disorder, etc.) accompanied by changes of the magnetic states of atoms.

DOI: 10.1103/PhysRevB.72.054441 PACS number(s): 75.50.Cc, 71.20.Lp, 71.15.Rf

I. INTRODUCTION

The Heusler alloys are the most prominent representatives of ternary compounds. Since 1903, when Heusler[1] first reported on ferromagnetic properties of the Cu_2MnAl compound, they are permanently attractive for many investigators due to the diverse magnetic phenomena.[2,3] Currently the Heusler alloys are at the focus of a large scientific interest due to their potential for applications in magnetic field sensors and spintronics devices.[4] For these purposes materials with a high spin polarization of carriers, so-called half-metallic ferromagnets,[5] are desirable, and many Heusler alloys seem to show this property.

The Heusler alloys are now defined as well-ordered ternary intermetallic compounds, at the stoichiometric composition X_2YZ, which have the cubic $L2_1$ structure. These compounds involve two different transition metal atoms X and Y and a third element Z which is a nonmagnetic metal or nonmetallic element. The numerous theoretical and experimental studies of Heusler alloys have been carried out, and it has been shown that composition and heat treatment are important parameters determining their magnetic properties.

Recently, a considerable attention is paid to Heusler compounds containing Co in the X sublattice.[6] Especially, the Co_2CrAl compound is the only one which preserves the nearly half-metallicity at the surface[7] whereas in other compounds the surface states kill the spin polarization at the Fermi level. However, some of the interfaces have been found to almost retain the half-metallicity.[8,9] The Co_2YZ are of particular interest because the magnetic moment per Co atom is known to have values ranging from $0.3\mu_B$ to $1.0\mu_B$ in these alloys.[10] It is considered that the magnetic moment on the Co atom depends strongly on the local environment.[11]

In order to achieve a desired modification of the electronic and magnetic properties, the doped Heusler alloys are intensively studied.[12–14] In the doped alloys the atoms in one of the sublattices are partly substituted by atoms of another element that may lead in some cases to qualitative changes of physical properties. For example, a large magnetoresistive effect of about 30% in a small magnetic field of 0.1 T at room temperature was recently observed[6,15] in $Co_2Cr_{0.6}Fe_{0.4}Al$ whereas the Co_2CrAl compound shows no effect.

The electronic and magnetic properties of Co_2CrAl and Co_2FeAl compounds as well as quaternary Heusler alloys $Co_2Cr_{1-x}Fe_xAl$ have been investigated using the first-principles calculation.[16–20] In Ref. 16 the origin of the half-metallicity in a series of Heusler alloys was discussed and it was shown that their total magnetic moment follows the Slater-Pauling behavior $M_t=Z_t-24$, where M_t is the total magnetic moment in μ_B per unit cell and Z_t is the total number of valence electrons. Galanakis[17] using the Korringa-Kohn-Rostoker method combined with the coherent potential approximation (KKR-CPA) formalism showed that the total spin moment in the quaternary Heusler alloy $Co_2Cr_{1-x}Fe_xAl$ varies linearly between Co_2CrAl and Co_2FeAl by varying the concentration of Cr and Fe. Miura *et al.*[18,19] investigated the effect of the atomic disorder on the half-metallicity of $Co_2Cr_{1-x}Fe_xAl$ compounds. They have shown that disorder between Cr and Al does not significantly reduce the spin polarization of the parent alloy Co_2CrAl, while disorder between Co and Cr makes a considerable reduction of the spin polarization. However, it has become clear that the disordering between the Co and Cr sites is unlikely to occur energetically. It was observed that the spin polarization of $Co_2Cr_{1-x}Fe_xAl$ decreases with increasing Fe concentration x in both the ordered $L2_1$ and the disordered $B2$ structures, and that the effects of the disorder on the spin polarization is significant at low Fe concentrations. Block *et al.*[20] studied

the effect of uniform strain and tetragonal distortion on the electronic and magnetic properties of Heusler compounds Co_2CrAl and NiMnSb using the self-consistent first-principle calculations. They show that the half-metallic character of the Heusler phases is lost with only a few percent uniform stress or tetragonal distortion of the lattice. The orbital magnetism in some half-metallic Heusler alloys including Co_2CrAl and Co_2FeAl have been studied recently by Galanakis[21] using the fully relativistic screened Korringa-Kohn-Rostoker (RKKR) method. It was found that the calculated orbital magnetic moments are negligible with respect to the spin moments, in contrast to the values obtained from the experimental x-ray magnetic circular dichroism (XMCD) spectra using sum rules.[22,23]

Besides theoretical investigations some important experimental results have been reported recently for the doped Heusler compounds $Co_2Cr_{1-x}Fe_xAl$ and related alloys.[22,24–26] References 22 and 24 reported the observation of the tunnel magnetoresistance at room temperature for the magnetic tunnel junction that utilizes $Co_2Cr_{0.6}Fe_{0.4}Al$ and Co_2MnAl, respectively, as an electrode. Reference 25 reported the observation of phase separation in $Co_2Cr_{1-x}Fe_xAl$.

In the present study, we focus our attention on the x-ray magnetic circular dichroism in the doped Heusler alloys $Co_2Cr_{1-x}Fe_xAl$. The XMCD technique developed in recent years has evolved into a powerful magnetometry tool to separate orbital and spin contributions to element specific magnetic moments. XMCD experiments measure the absorption of x rays with opposite (left and right) states of circular polarization. Recently x-ray magnetic circular dichroism in the ferromagnetic $Co_2Cr_{0.6}Fe_{0.4}Al$ alloy has been measured at the Co, Fe, and Cr $L_{2,3}$ edges.[23] Using the magneto-optic sum rules the orbital moments of Co, Fe, and Cr have been deduced to be 0.12, 0.33, and $0.04\mu_B$, respectively. The authors also have calculated the Co, Fe, Cr, and Al partial density of states for the $Co_2Fe_{0.5}Cr_{0.5}Al$ compound using the linear-muffin-tin-orbital (LMTO) band structure method in the atomic sphere approximation (ASA) to interpret the XMCD spectra. However, they do not include the spin-orbit (SO) interaction in their calculations and, hence, were not able to obtain the XMCD spectra as well as the orbital moments.

This paper is organized as follows. Section II presents a description of the doped Heusler alloys $Co_2Cr_{1-x}Fe_xAl$ crystal structure and the computational details. Section III is devoted to the electronic structure for Co_2CrAl and Co_2FeAl compounds and XMCD spectra of the doped Heusler alloy $Co_2Cr_{0.625}Fe_{0.375}Al$ calculated in the fully relativistic Dirac LMTO band structure method. We also present the theoretical calculations of the Kerr spectra of Co_2FeAl compound. The calculated results are compared with the available experimental data. Finally, the results are summarized in Sec. IV.

II. CRYSTAL STRUCTURE AND COMPUTATIONAL DETAILS

The Heusler-type X_2YZ compound crystallized in the cubic $L2_1$ structure with $Fm\bar{3}m$ symmetry (No. 225) is formed by four interpenetrating fcc sublattices. The X ions occupy the $4b$ Wyckoff positions ($x=\frac{1}{4}$, $y=\frac{1}{4}$, $z=\frac{1}{4}$). The Y ions occupy the $4a$ positions ($x=0$, $y=0$, $z=0$), and the Z ions are placed at the $4b$ sites ($x=\frac{1}{2}$, $y=\frac{1}{2}$, $z=\frac{1}{2}$). Both the X and Y atoms have eight nearest neighbors at the same distance. Y atom has eight X atoms as nearest neighbors, while for X there are four Y and four Z atoms.

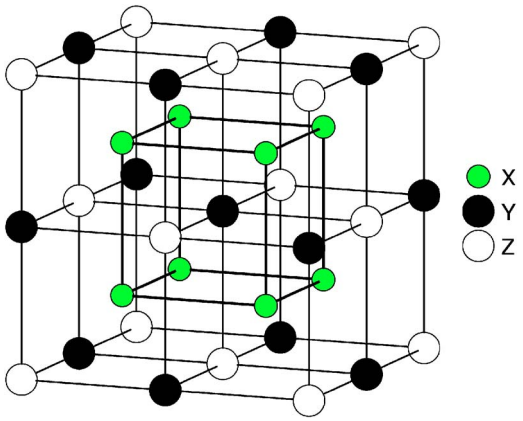

FIG. 1. (Color online) Schematic representation of the $L2_1$ structure. The cubic cell contains four primitive cells.

In order to simulate the structures where the Y sublattice is occupied by both Fe and Cr atoms, we have considered the lattice with tetragonal cells that are formed by two cubic cells shown in Fig. 1. The tetragonal cell contains eight sites of the Y sublattice, and in this way it is possible to construct the systems $Co_2Cr_{1-x}Fe_xAl$ where x is equal to 0.125, 0.25, 0.375, etc.

We now turn to a description of the magneto-optical effects, which refer to various changes in the polarization state of light upon interaction with materials possessing a net magnetic moment, including rotation of the plane of linearly polarized light (Faraday, Kerr rotation), and the complementary differential absorption of left and right circularly polarized light (circular dichroism). In the near visible spectral range these effects result from excitation of electrons in the conduction band. Near x-ray absorption edges, or resonances, magneto-optical effects can be enhanced by transitions from well-defined atomic core levels to valence states selected by transition matrix element symmetry. There are at least two alternative formalisms for describing resonant x-ray magneto-optical (MO) properties. One approach uses the classical dielectric tensor.[27] Another one uses the resonant atomic scattering factor including charge and magnetic contributions.[28,29] The equivalence of these two descriptions (within dipole approximation) is demonstrated in Ref. 30.

Using straightforward symmetry considerations it can be shown that all magneto-optical phenomena (XMCD, MO Kerr and Faraday effects) are caused by the symmetry reduction, in comparison to the paramagnetic state, caused by magnetic ordering.[31] This symmetry lowering has consequences only when SO coupling is considered in addition. Therefore, in order to calculate the XMCD properties one must account for both magnetism and SO coupling at the same time when dealing with the electronic structure of the material considered.

For the polar Kerr magnetization geometry and a crystal of tetragonal symmetry, where both the fourfold axis and the magnetization **M** are perpendicular to the sample surface and the z axis is chosen to be parallel to them, the dielectric tensor is composed of the diagonal ε_{xx} and ε_{zz}, and the off-diagonal ε_{xy} components and has the form

$$\varepsilon = \begin{pmatrix} \varepsilon_{xx} & \varepsilon_{xy} & 0 \\ -\varepsilon_{xy} & \varepsilon_{xx} & 0 \\ 0 & 0 & \varepsilon_{zz} \end{pmatrix}. \tag{1}$$

In the polar geometry the expression for the complex Kerr angle can be easily obtained for small angles and is given by[32]

$$\theta_K(\omega) + i\varepsilon_K(\omega) = -\sigma_{xy}(\omega)/D(\omega), \tag{2}$$

where

$$D(\omega) = \sigma_{xx}(\omega)\sqrt{1 + \frac{4\pi i}{\omega}\sigma_{xx}(\omega)}, \tag{3}$$

with θ_K being the Kerr rotation and ε_K being the so-called Kerr ellipticity. $\sigma_{\alpha\beta}$ $(\alpha,\beta \equiv x,y,z)$ is the optical conductivity tensor, which is related to the dielectric tensor $\varepsilon_{\alpha\beta}$ through

$$\varepsilon_{\alpha\beta}(\omega) = \delta_{\alpha\beta} + \frac{4\pi i}{\omega}\sigma_{\alpha\beta}(\omega). \tag{4}$$

The optical conductivity tensor components, or equivalently, the dielectric tensor are the basic spectral quantities of the medium and can be evaluated from the optical and Kerr effect measurements. The optical conductivity can be computed from the energy band structure by means of the Kubo-Greenwood[33] linear-response expression,[34]

$$\sigma_{\alpha\beta}(\omega) = \frac{-ie^2}{m^2\hbar V_{uc}} \sum_{\mathbf{k}} \sum_{nn'} \frac{f(\epsilon_{n\mathbf{k}}) - f(\epsilon_{n'\mathbf{k}})}{\omega_{nn'}(\mathbf{k})} \frac{\Pi^{\alpha}_{n'n}(\mathbf{k})\Pi^{\beta}_{nn'}(\mathbf{k})}{\omega - \omega_{nn'}(\mathbf{k}) + i/\tau}, \tag{5}$$

with $f(\epsilon_{n\mathbf{k}})$ the Fermi function, $\hbar\omega_{nn'}(\mathbf{k}) \equiv \epsilon_{n\mathbf{k}} - \epsilon_{n'\mathbf{k}}$, the energy difference of the Kohn-Sham energies $\epsilon_{n\mathbf{k}}$, and $\gamma \equiv \tau^{-1}$ is the lifetime parameter, which is included to describe the finite lifetime of excited Bloch electron states. $\Pi^{\alpha}_{nn'}$ are the dipolar optical transition matrix elements, which in a fully relativistic description are given by

$$\Pi_{nn'}(\mathbf{k}) = \langle \Psi_{n\mathbf{k}} | c\boldsymbol{\alpha} | \Psi_{n'\mathbf{k}} \rangle, \tag{6}$$

where $\Psi_{n\mathbf{k}}$ is the four-component Bloch electron wave function, $\boldsymbol{\alpha}$ are Dirac matrices.

Expression (5) for the conductivity contains a double sum over all energy bands, which naturally separates in the so-called interband contribution, i.e., $n \neq n'$, and the intraband contribution, $n = n'$. The intraband contribution to the diagonal components of $\boldsymbol{\sigma}$ may be rewritten for zero temperature as[35]

$$\sigma_{\alpha\alpha}(\omega) \equiv \frac{(\omega_{p,\alpha})^2}{4\pi} \frac{i}{\omega + i\gamma_D}, \tag{7}$$

with $\omega_{p,\alpha}$ the components of the plasma frequency. Equation (7) is identical to the classical Drude result for the ac conductivity, with $\gamma_D = 1/\tau_D$, and τ_D the phenomenological Drude electron relaxation time. The intraband relaxation time parameter γ_D may be different from the interband relaxation time parameter γ. The latter can be frequency dependent,[36] and, because excited states always have a finite lifetime, will be nonzero, whereas γ_D will approach zero for very pure materials.

Within the one-particle approximation, the absorption coefficient μ for incident x-ray of polarization λ and photon energy $\hbar\omega$ can be determined as the probability of electron transitions from an initial core state (with wave function Ψ_j and energy E_j) to a final unoccupied states (with wave functions $\Psi_{n\mathbf{k}}$ and energies $E_{n\mathbf{k}}$),[35]

$$\mu_j^{\lambda}(\omega) = \sum_{n\mathbf{k}} |\langle \Psi_{n\mathbf{k}} | \mathcal{J}_{\lambda} | \Psi_j \rangle|^2 \delta(E_{n\mathbf{k}} - E_j - \hbar\omega)\theta(E_{n\mathbf{k}} - E_F), \tag{8}$$

with $\mathcal{J}_{\lambda} = -e\boldsymbol{\alpha}\mathbf{a}_{\lambda}$ being the dipole electron-photon interaction operator, where $\mathbf{a}_{\lambda}$ is the λ polarization unit vector of the photon vector potential $[a_{\pm} = 1/\sqrt{2}(1, \pm i, 0), a_z = (0,0,1)]$. (Here $+/-$ denotes, respectively, left and right circular photon polarizations with respect to the magnetization direction in the solid.)

In order to simplify the comparison of the theoretical x-ray isotropic absorption spectra to the experimental ones we take into account the background intensity which affects the high energy part of the spectra. The shape of x-ray absorption caused by the transitions from inner levels to the continuum of unoccupied levels was first discussed by Richtmyer *et al.* in the early 1930s.[37] The absorption coefficient with the assumption of equally distributed empty continuum levels is

$$\mu(\omega) = \frac{C\Gamma_c}{2\pi} \int_{E_{cf_0}}^{\infty} \frac{dE_{cf}}{(\Gamma_c/2)^2 + (\hbar\omega - E_{cf})^2}, \tag{9}$$

where $E_{cf} = E_c - E_f$, E_c and Γ_c are the energy and the width of a core level, E_f is the energy of empty continuum level, E_{f_0} is the energy of the lowest continuum level, and C is a normalization constant which has been used as an adjustable parameter.

Concurrent with the x-ray magnetic circular dichroism experimental developments, some important magneto-optical sum rules have been derived in recent years.[38–41]

For the $L_{2,3}$ edges the l_z sum rule can be written as[35]

$$\langle l_z \rangle = n_h \frac{4\int_{L_3+L_2} d\omega(\mu_+ - \mu_-)}{3\int_{L_3+L_2} d\omega(\mu_+ + \mu_-)}, \tag{10}$$

where n_h is the number of holes in the d band $n_h = 10 - n_d$, $\langle l_z \rangle$ is the average of the magnetic quantum number of the orbital

angular momentum. The integration is taken over the whole $2p$ absorption region. The s_z sum rule is written as

$$\langle s_z \rangle + \frac{7}{2}\langle t_z \rangle = n_h \frac{\int_{L_3} d\omega(\mu_+ - \mu_-) - 2\int_{L_2} d\omega(\mu_+ - \mu_-)}{\int_{L_3+L_2} d\omega(\mu_+ + \mu_-)}, \tag{11}$$

where t_z is the z component of the magnetic dipole operator $\mathbf{t}=\mathbf{s}-3\mathbf{r}(\mathbf{r}\cdot\mathbf{s})/|\mathbf{r}|^2$ which accounts for the asphericity of the spin moment. The integration $\int_{L_3}$ ($\int_{L_2}$) is taken only over the $2p_{3/2}$ ($2p_{1/2}$) absorption region.

The details of the computational method are described in our previous papers,[42–44] and here we only mention several aspects. The calculations (corresponding to zero temperature) were performed for the experimentally observed lattice constants, using the spin-polarized fully relativistic linear-muffin-tin-orbital (SPR LMTO) method[45,46] in the atomic sphere approximation (ASA) with the combined correction term taken into account. The calculations was based on the local spin-density approximation (LSDA) with the Perdew-Wang[47] parametrization of the exchange-correlation potential. Brillouin zone (BZ) integrations were performed using the improved tetrahedron method[48] and charge self-consistency was obtained on a grid of 349 **k** points in the irreducible part of the BZ. The basis consisted of transition metal s, p, d, and f and Al s, p, and d LMTO's.

The measured cubic lattice constant of Co_2FeAl is equal to 0.5730 nm.[49,50] For Co_2CrAl however the published respective data are confusing, $a=0.5887$ nm (Ref. 49) and $a=0.5727$ nm (Ref. 50). Unfortunately, these quite different values were transferred to reviews and handbooks, the first one can be found in Ref. 2, the second one in Ref. 51, and both in Ref. 52. The recent x-ray diffraction measurements[53] indicate the value of $a=(0.574\pm0.003)$ nm for Co_2CrAl compound. Also the recently measured lattice constant of $Co_2Cr_{0.6}Fe_{0.4}Al$ compound ($a=0.5737$ nm) (Ref. 23) confirms that both Co_2FeAl and Co_2CrAl compounds have almost the same lattice spacing. In the present calculations we have used the value of 0.5730 nm for the lattice constants of all compositions considered.

In our magneto-optical calculations we adopt the perfect crystal approximation, i.e., $\gamma_D \to 0$. For the interband relaxation parameter we used $\gamma=0.4$ eV. The Kramers-Kronig transformation has been used to calculate the dispersive parts of the optical conductivity from the absorptive parts.

Finally, the intrinsic broadening mechanisms have been accounted for by folding XMCD spectra with a Lorentzian. For the finite lifetime of the core hole a constant width Γ_c, in general from Ref. 54, has been used. The finite apparative resolution of the spectrometer has been accounted for by a Gaussian of 0.4 eV.

III. RESULTS AND DISCUSSION

A. Results for Co_2CrAl and Co_2FeAl

(a) *Energy band structure:* The total and partial DOS's of Co_2CrAl are presented in Fig. 2. The results agree well with previous band structure calculations.[7,16,18,20] The occupied part of the valence band can be subdivided into several regions. Al $2s$ states appear between −10.0 and −6.0 eV. The energy states in the energy range −6.0 to 2.0 eV are formed mainly by Co and Cr d states. Our calculations show that Co_2CrAl has local magnetic moments of $0.720\mu_B$ on Co and $1.602\mu_B$ on Cr. The orbital moments are equal to $0.013\mu_B$ and $0.008\mu_B$ on the Co and Cr sites, respectively. The results are in good agreement with recent RKKR calculations.[21] The interaction between the transition metals is ferromagnetic, leading to a total calculated moment of $2.970\mu_B$.

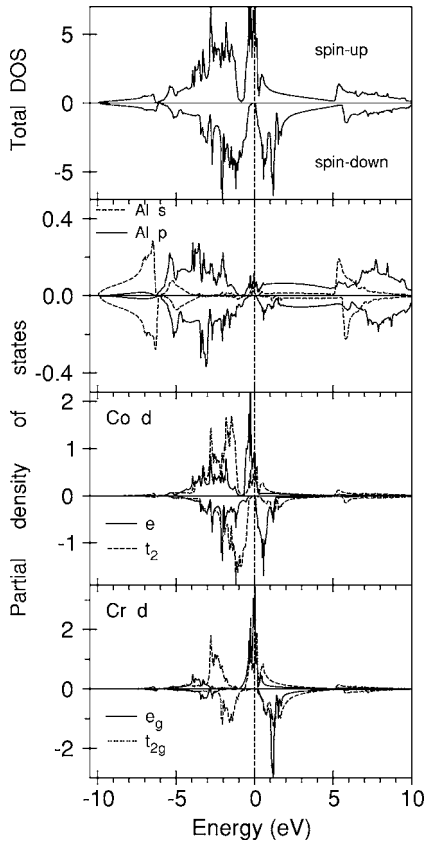

FIG. 2. The total [in states/(cell eV)] and partial [in states/(atom eV)] density of states of Co_2CrAl.

The crystal field at the Co $4b$ site (T_d point symmetry) causes the splitting of d orbitals into a doublet e ($3z^2-1$ and x^2-y^2) and a triplet t_2 (xy, yz, and xz). The crystal field at the Cr $4a$ site (O_h point symmetry) splits Cr d states into e_g ($3z^2-1$ and x^2-y^2) and t_{2g} (xy, yz, and xz) ones. The hybridization between Cr and Co d states plays an important role in the formation of the band structure of Co_2CrAl. It leads to the splitting of the d states into the bonding states which have predominantly Co d character and the antibonding states with stronger contribution of Cr d states. The majority and minority spin bonding states are found below −2 eV and −0.5 eV, respectively.

It is important to note, that the antibonding Cr d–Co d states form a sharp peak in the DOS of the majority-spin electrons at the Fermi level. The presence of the peak at E_F can be responsible for the antisite disorder in Co_2CrAl. Indeed, Miura *et al.*[18] show that the disorder of Cr-Co or

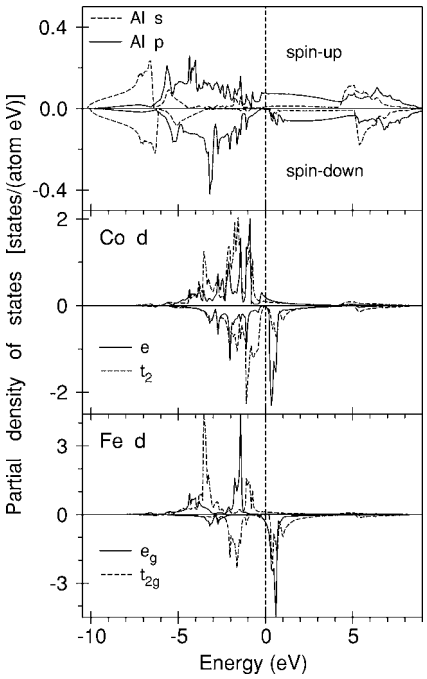

FIG. 3. The spin and symmetry projected partial density of states of Co_2FeAl.

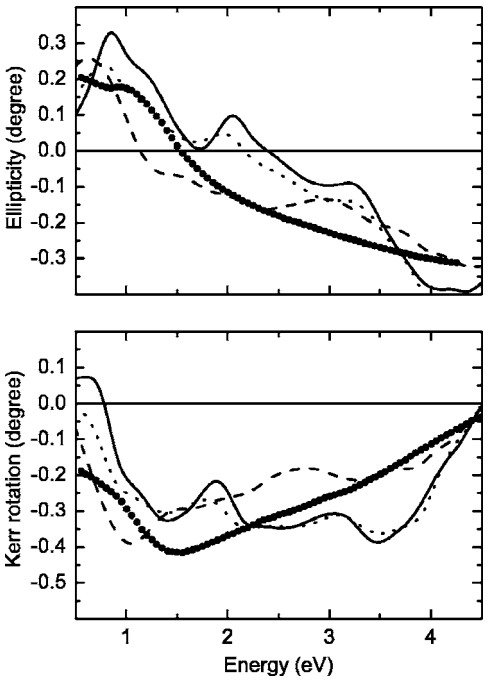

FIG. 4. Calculated polar Kerr rotation (lower panel) and ellipticity (upper panel) spectra of the Co_2FeAl compound having a perfect lattice (solid line) and containing vacancies (dashed line) and Co atoms as antisite defects (dotted line) in the Fe sublattice. Theoretical results are compared with the experimental spectra (solid circles) taken from Ref. 51.

Cr-Al types leads to a considerable reduction of the corresponding peak in the Cr partial DOS at the Fermi level.

The strong hybridization between the minority spin Cr d and Co d states leads to the opening of a gap of 0.18 eV. Thus, according to the spin-polarized calculations Co_2CrAl is a half-metallic ferromagnet if the spin-orbit coupling is neglected. Although spin-orbit splitting of the d energy bands for both the Co and Cr atoms is much smaller than their spin and crystal-field splittings this interaction destroys the energy gap for the minority spin states. The Fermi level falls within a region of very small but finite minority-spin DOS. In this case the spin polarization of electron states at the Fermi energy is equal to 98%. Similar results were obtained in Refs. 55 and 56 for some other Heusler alloys. Authors show that the spin-orbit interaction can cause a nonvanishing density of states within the minority-spin band gap of half-metals around the Fermi level and reduce the spin polarization at the E_F.

It is important to note that there is a hybridization quasi-gap in DOS at around 5 eV above Fermi level (Fig. 2) due to transition metal d-Al sp hybridization. This feature is typical for the whole series of Heusler alloys $Co_2Cr_{1-x}Fe_xAl$ and is reflected in corresponding transition metal $L_{2,3}$ x-ray absorption spectra (see below).

Figure 3 shows the spin and symmetry projected partial densities of states of Co_2FeAl. Co_2FeAl has local magnetic moments of $1.106\mu_B$ on Co and $2.695\mu_B$ on Fe. The orbital moments are equal to $0.047\mu_B$ and $0.064\mu_B$ on Co and Fe, respectively. The interaction between the transition metals is ferromagnetic, leading to a total calculated moment of $4.811\mu_B$.

The energy of Fe d states is lower than the energy of Cr d ones and, in contrast to Co_2CrAl, majority spin Co and Fe d states in Co_2FeAl are almost completely occupied. The center of the majority spin Fe d states is shifted below the corresponding Co states because of the stronger exchange interaction in the Fe d shell. As a consequence there is no gap between bonding and antibonding Co d–Fe d states.

Similar to Co_2CrAl the minority spin d states are split into well separated bonding and antibonding states, the latter being unoccupied. However, the gap between the bonding and antibonding states is closed and the density of states at E_F is small but finite. Thus, even if the spin-orbit coupling is neglected, Co_2FeAl does not exhibit a half-metallic behavior.

(b) *MO spectra:* Let us consider now the magneto-optical properties of Co_2CrAl and Co_2FeAl compounds. The Kerr rotation and ellipticity measurements have been done in Refs. 50 and 51. For Co_2CrAl the measured Kerr rotation θ_K in the energy range between 1.5 and 2.0 eV is equal only to −0.01 degree in excellent agreement with our calculations. In Co_2FeAl the Kerr rotation in this energy range is about −0.4 degree. Also for this compound the agreement between experiment and calculations is rather good both in the Kerr rotation and ellipticity (see Fig. 4).

Additionally we have studied effects of some kinds of point defects on the magnetic and magneto-optical properties of Co_2FeAl. If one of eight Fe atoms in the tetragonal cell is substituted by a Co atom, the shape of the magneto-optical spectra changes only slightly. It follows from the calculations that the Co impurity in the Fe sublattice is forced to increase its local magnetic moments up to $M_s=1.531\mu_B$ and $M_l=0.113\mu_B$. These values are much closer to those ones characteristic for the Co metal, as one would expect due to eight *official* Co atoms that are the nearest surrounding of the Co impurity.

TABLE I. Calculated local magnetic moments (in μ_B) of Co atoms that have different nearest atomic surrounding in the doped compounds $Co_2Cr_{1-x}Fe_xAl$. For each configuration the range of x values is given, where this configuration is present in the structure models used in our calculations.

Surrounding of Co atom	Range of x	M_s		M_l
		min	max	
4 Cr	(0.0, 0.250)	0.713	0.721	0.014
3 Cr+1 Fe	(0.125, 0.375)	0.821	0.847	0.024
2 Cr+2 Fe	(0.250, 0.750)	0.924	0.961	0.033
1 Cr+3 Fe	(0.625, 0.875)	1.011	1.013	0.041
4 Fe	(0.750, 1.0)	1.106	1.110	0.048

If vacancies are created in the Co_2FeAl structure by removing one Fe atom in the tetragonal cell, the effect on the magneto-optical spectra is quite strong. The energy dependence of the Kerr rotation and ellipticity becomes more smooth and the overall shape of the curves is closer to the experimental ones. Note, that the vacancies destroy the feature at 3.5 eV in the Kerr rotation that is observed experimentally for the Co metal and is very sensitive to the hybridization of the valence-band electron states in the Co-based systems with other transition metals.[57,58] It can also be assumed to be a Fe deficiency in samples used to obtain the presented experimental results.[51] The Co atoms surrounding the vacancy in the Fe sublattice are significantly affected by this defect. The local magnetic moments of these Co atoms are decreased in comparison to those in the perfect lattice, $M_s=0.784\mu_B$ and $M_l=0.039\mu_B$. The vacancy site itself has a small spin magnetic moment of the opposite sign ($M_s=-\mu_B$) induced by extended valence-band electron states.

B. Doped compounds $Co_2Cr_{1-x}Fe_xAl$

(c) *Electronic structure:* We have calculated the electronic and magnetic structures as well as the XMCD spectra of the pseudoternary Heusler series $Co_2Cr_{1-x}Fe_xAl$ for $x=0$ 0.125, 0.25, 0.375, 0.5, 0.675, 0.75, and 1. For the calculations of the doped compounds $Co_2Cr_{1-x}Fe_xAl$ the configurations of Cr and Fe atoms were chosen that are the most symmetrical ones for the given value of x.

Our calculations show that the spin polarization of the electron states at the Fermi level for mixed compounds has quite a high value above 95% with x varying from $x=0$ up to $x=0.4$, and then it decreases rather abruptly. This result, in fact, supports the conclusion already drawn in Ref. 18. The spin-orbit interaction taken into account in the fully relativistic calculations reduces the spin polarization at the Fermi level, and this effect becomes more pronounced with increasing Fe content.

The comparison of calculated results obtained for different Fe contents in the doped compounds shows that the local magnetic moments are determined rather by the kind of the atomic surrounding than by the actual value of x. As can be seen from Table I, the local magnetic moments of Co atoms are very close to each other if the nearest surrounding of Co atoms is the same in the different doped compounds. We have presented in Table I the maximal and minimal values of M_s from all calculated ones for the given local atomic configuration. The differences in the M_l values do not exceed 0.001.

The spin magnetic moment of Fe atoms varies in different doped compounds from $2.695\mu_B$ to $2.808\mu_B$ and depends mainly on the Fe-Fe distance. Comparison of calculated results for different local atomic configurations in various doped compounds shows that the maximal value of M_s is reached if there are no other Fe atoms in the vicinity of the considered Fe atom, and this value decreases with the number of Fe neighbors in the Y sublattice. The calculated orbital magnetic moment of Fe atoms lies between $0.061\mu_B$ (small x) and $0.064\mu_B$ (x approaching to 1).

The magnetic states of Cr atoms were found to be very sensitive to the local atomic surrounding, although the variations of M_s are relatively small (between $1.518\mu_B$ and $1.618\mu_B$). It should be noted, that the calculated values of M_l may have opposite signs even in the same doped compound if the Cr atoms occupy nonequivalent positions in the Y sublattice. The orbital magnetic moments of Cr atoms vary from $-0.015\mu_B$ to $0.018\mu_B$. Comparing these values of M_s and M_l with those for the Co_2CrAl compound, one can see that the doping with Fe atoms leads either to increasing or to decreasing local magnetic moments of Cr atoms. Unfortunately, we have not found clear trends in the formation of the Cr magnetic moments like those ones observed for Fe atoms. It is only determined that the Cr magnetic moments strongly depend not only on the kind of surrounding atoms but also on the arrangement of these atoms around the Cr atom.

It can be concluded from the calculated results that the local magnetic state of Fe atoms is the most stable one in the doped compounds. It strongly influences the magnetic states of Co and Cr atoms and plays therefore the leading role in the formation of the magnetic properties of these compounds.

A large magnetoresistance of about 30% observed[6,15] in the Heusler alloy $Co_2Cr_{0.6}Fe_{0.4}Al$ is evidently caused by the presence of doped Fe atoms since no significant magnetoresistive effects were found in Co_2CrAl. It could be supposed that the doped compound with $x\approx 0.4$ may be really optimal for technological applications because of a significant Fe content in combination with a high spin polarization of electron states at the Fermi level.

Figure 5 shows the spin and symmetry projected partial density of states of $Co_2Cr_{1-x}Fe_xAl$ with $x=0.375$. In the

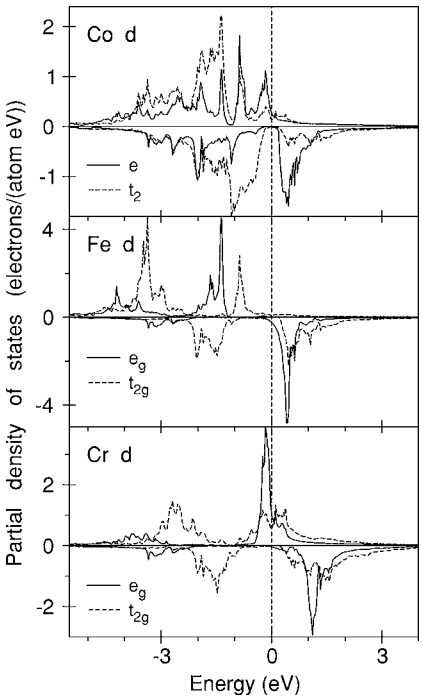

FIG. 5. The spin and symmetry projected partial density of states of $Co_2Cr_{0.625}Fe_{0.375}Al$ compound.

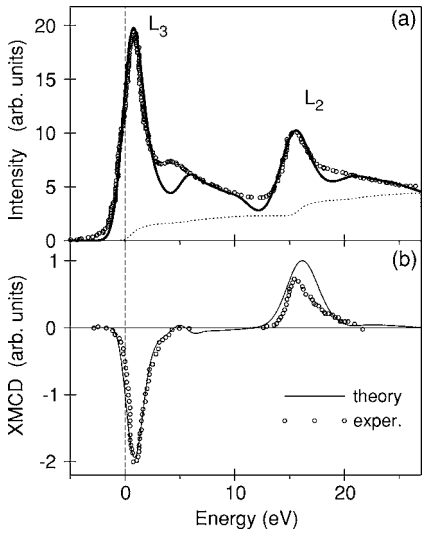

FIG. 6. Calculated (thick full line) and experimental (circles) isotropic absorption (a) and XMCD spectra (b) of $Co_2Cr_{0.625}Fe_{0.375}Al$ compound at the Co $L_{2,3}$ edges. Experimental spectra (Ref. 23) were measured with external magnetic field (0.3 T) for the quenched sample. The upper panel also shows the background spectra (dotted line) due to the transitions from inner $2p_{1/2,3/2}$ levels to the continuum of unoccupied levels (Ref. 37).

model structure there are three nonequivalent positions for Fe atoms, and two nonequivalent positions for each Co and Cr atoms. We found that the Co as well as Fe partial DOS's are quite similar for the different types. However, Cr(1) and Cr(2) atoms have visible difference in the energy distribution of d_{e_g} states in the vicinity of the Fermi level.

(d) *XMCD spectra:* At the core level edge XMCD is not only element specific but also orbital specific. For $3d$ transition metals, the electronic states can be probed by the K, $L_{2,3}$, and $M_{2,3}$ x-ray absorption and emission spectra.

Recently x-ray magnetic circular dichroism in the ferromagnetic $Co_2Cr_{0.6}Fe_{0.4}Al$ alloy has been measured at the Co, Fe, and Cr $L_{2,3}$ edges.[23] Due to the differences in the magnetic states of atoms that occupy nonequivalent positions in the lattice of the doped compound, the interpretation of the experimental results with the aim to determine the local magnetic moments becomes a nontrivial problem because in the experiment a superposition of signals from magnetically different atoms is measured.

To explain the experimental XMCD spectra of $Co_2Cr_{0.6}Fe_{0.4}Al$ alloy we calculated the electronic structure, x-ray absorption and XMCD spectra for the compound $Co_2Cr_{1-x}Fe_xAl$ with $x=0.375$ using fully relativistic spin-polarized LMTO method.

The experimentally measured dichroic lines have different signs at the L_3 and L_2 edges of Co, Fe, and Cr.[59] In order to compare relative amplitudes of the L_3 and L_2 XMCD spectra we first normalize the corresponding isotropic x-ray absorption spectra (XAS) to the experimental ones taking into account the background scattering intensity as described in Sec. II. Figure 6 shows the calculated isotropic x-ray absorption and XMCD spectra at the $L_{2,3}$ edges of Co in the LSDA approach together with the experimental data.[23] The contribution from the background scattering is shown by the dotted line in the upper panel of Fig. 6. The two nonequivalent Co ions produce similar XAS's with almost identical energy positions and intensities, therefore we present in Fig. 6 XAS and XMCD spectra as a sum over the nonequivalent atoms.

Because of the dipole selection rules, apart from the $4s_{1/2}$ states (which have a small contribution to the XAS due to relatively small $2p \rightarrow 4s$ matrix elements) only $3d_{3/2}$ states occur as final states for L_2 XAS for unpolarized radiation, whereas for the L_3 XAS $3d_{5/2}$ states also contribute.[35] Although the $2p_{3/2} \rightarrow 3d_{3/2}$ radial matrix elements are only slightly smaller than for the $2p_{3/2} \rightarrow 3d_{5/2}$ transitions the angular matrix elements strongly suppress the $2p_{3/2} \rightarrow 3d_{3/2}$ contribution.[35] Therefore neglecting the energy dependence of the radial matrix elements, the L_2 and the L_3 spectrum can be viewed as a direct mapping of the DOS curve for $3d_{3/2}$ and $3d_{5/2}$ character, respectively.

The experimental Co XAS has a pronounced shoulder at the L_3 peak shifted by about 4 eV with respect to the maximum to a higher photon energy. This structure is less pronounced at the L_2 edge. This result can be ascribed to the lifetime broadening effect because the lifetime of the $2p_{1/2}$ core hole is shorter than the $2p_{3/2}$ core hole due to the L_2L_3V Coster-Kronig decay. This feature is partly due to the interband transitions from the $2p$ core level to $3d$ empty states at around 4.7–5.5 eV just above the quasigap (Fig. 7). On the other hand, analyzing the upper panel of Fig. 6 we can conclude that the experimentally measured Co L_3 XAS still has an additional intensity around 4 eV which is not produced by the theoretical calculations. The feature is reproduced theoretically also at the Fe and Cr L_3 edges (see Figs. 8 and 9). Although the structure is less pronounced in these cases it also cannot be fully reproduced by the theoretical calculations. It might be indicated that an additional satellite struc-

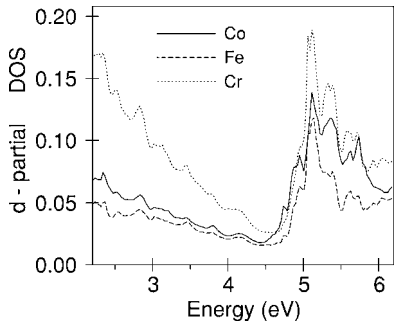

FIG. 7. The Co, Fe, and Cr *d*-partial density of unoccupied states [in states/(atom eV)] of $Co_2Cr_{0.625}Fe_{0.375}Al$.

ture can affect the high energy tails of the Co, Fe, and Cr $L_{2,3}$ XAS's. This question needs an additional theoretical investigation using an appropriate many-body treatment.

The XMCD spectra at the $L_{2,3}$ edges are mostly determined by the strength of the SO coupling of the initial $2p$ core states and spin polarization of the final empty $3d_{3/2,5/2}$ states while the exchange splitting of the $2p$ core states as well as the SO coupling of the $3d$ valence states are of minor importance for the XMCD at the $L_{2,3}$ edge of $3d$ transition metals.[35] The calculated Co $L_{2,3}$ XMCD spectra are in good agreement with the experiment, although the calculated magnetic dichroism is somewhat too high at the L_2 edge. The main reason for this discrepancy is the core-hole effect. When the $2p$ core electron is photoexcited to the unoccupied d states, the distribution of the charge changes to account for the hole created. This effect is not taken into account by the method we used for the electronic structure calculations, and it is likely to lead to the observed discrepancy.[60]

It should be noted, that for Fe atoms we have not found noticeable differences in the shape of the XMCD spectra for

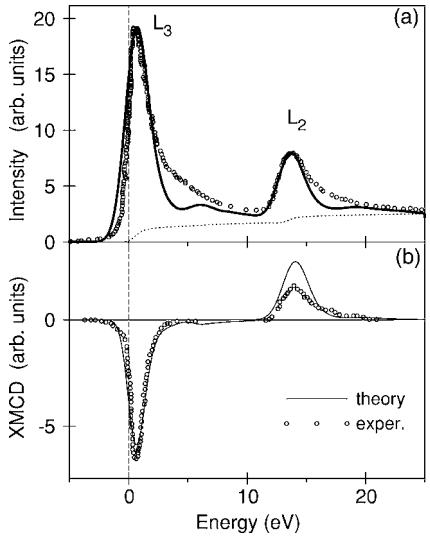

FIG. 8. Calculated (thick full line) and experimental (circles) (Ref. 23) isotropic absorption (a) and XMCD spectra (b) of the $Co_2Cr_{0.625}Fe_{0.375}Al$ compound at the Fe $L_{2,3}$ edges. The upper panel also shows the background spectra (dotted line) due to the transitions from the inner $2p_{1/2,3/2}$ levels to the continuum of unoccupied levels (Ref. 37).

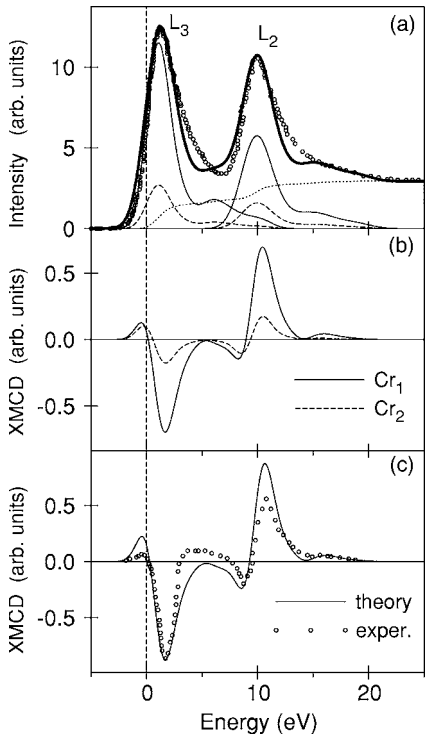

FIG. 9. Calculated (thick full line) and experimental (circles) (Ref. 23) isotropic absorption (a) and XMCD spectra (b) and (c) of the $Co_2Cr_{0.625}Fe_{0.375}Al$ compound at the Cr $L_{2,3}$ edges. The upper panel also shows the background spectra (dotted line) due to the transitions from the inner $2p_{1/2,3/2}$ levels to the continuum of unoccupied levels (Ref. 37). Full and dashed lines present the spectra for Cr_1 Cr_2, respectively.

atoms occupying nonequivalent positions, therefore we present in Fig. 8 the Fe XAS and XMCD $L_{2,3}$ spectra as a sum over all three nonequivalent atoms. The agreement between theory and the experiment is similar as it was found previously in the Co (Fig. 6).

Figure 9 presents the calculated isotropic absorption as well as XMCD spectra of the $Co_2Cr_{0.625}Fe_{0.375}Al$ compound at the Cr $L_{2,3}$ edges compared with the experimental data measured in the $Co_2Cr_{0.6}Fe_{0.4}Al$ alloy.[23] The theoretical results are given for 4 Cr(1) and 1 Cr(2) atoms. A small disagreement in the amplitude of the spectra at around 3 to 7 eV might be caused by possible disorder in the occupation of the Y sublattice by Cr and Fe atoms in the real structure of this compound.

To investigate the influence of the initial state on the resulting XMCD spectra we calculated also the XAS and XMCD spectra of the $Co_2Cr_{0.625}Fe_{0.375}Al$ alloy at the $M_{2,3}$ edges. The magnetic dichroism at the $M_{2,3}$ edge is much smaller than at the $L_{2,3}$ edge (Fig. 10). Besides the M_2 and the M_3 spectra are strongly overlapped due to the small spin-orbit splitting of the $3p$ core levels; the M_3 spectrum contributes to some extent to the structure of the total $M_{2,3}$ spectrum in the region of the M_2 edge. To decompose a corresponding experimental $M_{2,3}$ spectrum into its M_2 and M_3 parts will therefore be quite difficult in general.

We calculated also the XAS and XMCD spectra of Co, Fe, and Cr at the K edges. Figure 11 shows the calculated

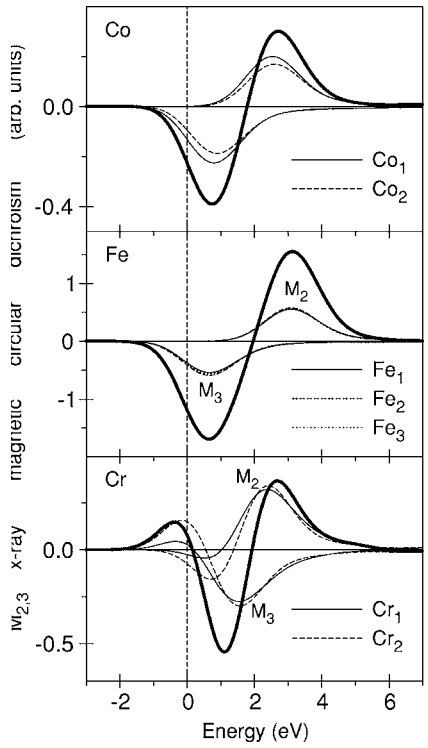

FIG. 10. The calculated XMCD spectra of the $Co_2Cr_{0.625}Fe_{0.375}Al$ compound at the Co, Fe, and Cr $M_{2,3}$ edges (thick full lines show the sum of the spectra at the M_3 and M_2 edges and all the nonequivalent atoms).

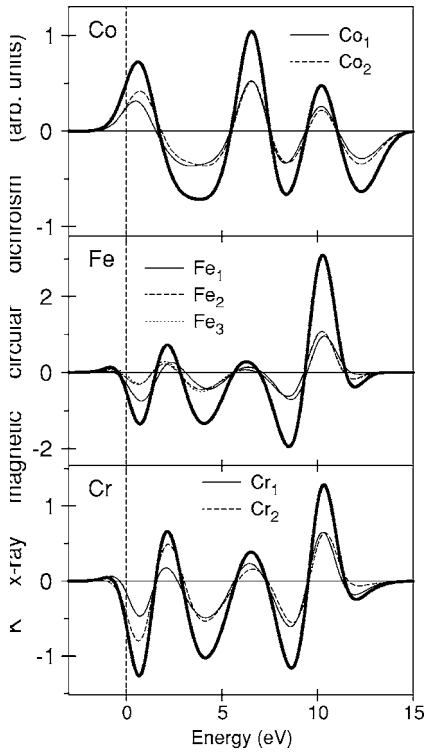

FIG. 11. The calculated XMCD spectra (multiplied by factor 10^3) of the $Co_2Cr_{0.625}Fe_{0.375}Al$ compound at the Co, Fe, and Cr K edges (thick full lines show the sum of the spectra for all nonequivalent atoms).

XMCD in terms of the difference in absorption $\Delta\mu_K=\mu_K^+-\mu_K^-$ for the left and right circularly polarized radiation. Because dipole allowed transitions dominate the absorption spectrum for unpolarized radiation, the absorption coefficient $\mu_K^0(E)$ (not shown) reflects primarily the DOS of the corresponding unoccupied $4p$-like states $N_p(E)$ above the Fermi level. Due to the energy dependent radial matrix element for the $1s\rightarrow 4p$ there is no strict one-to-one correspondence between $\mu_K(E)$ and $N_p(E)$. The exchange splitting of the initial $1s$-core state is extremely small[61] therefore only the exchange and spin-orbit splitting of the final $4p$ states is responsible for the observed dichroism at the K edge. For this reason the dichroism is found to be very small (Fig. 11).

(e) *Magnetic moments:* In magnets, the atomic spin M_s and orbital M_l magnetic moments are basic quantities and their separate determination is therefore important. Methods of their experimental determination include traditional gyromagnetic ratio measurements,[62] magnetic form factor measurements using neutron scattering,[63] and magnetic x-ray scattering.[64] In addition to these, the recently developed x-ray magnetic circular dichroism combined with several sum rules[38–41] has attracted much attention as a method of site- and symmetry-selective determination of M_s and M_l. Table II presents the comparison between calculated and experimental magnetic moments in $Co_2Cr_{0.625}Fe_{0.375}Al$. The spin magnetic moment at the Al site is very small and has an opposite direction to the spin moment at transition metal sites.

It is interesting to compare the spin and orbital moments obtained from the theoretically calculated XAS and XMCD spectra through sum rules [Eqs. (10) and (11)] with directly calculated LSDA values. In this case we at least avoid all the experimental problems. A similar comparison between the LSDA calculated magnetic moments and the ones derived by applying the sum rules to the theoretical spectra has been previously carried out also for the half-Heusler alloys.[65] The number of the transition metal $3d$ electrons is calculated by integrating the occupied d partial density of states inside the corresponding atomic sphere which gives the values averaged for the nonequivalent sites $n_{Co}=7.749$, $n_{Fe}=6.540$, and $n_{Cr}=4.567$. Sum rules reproduce the spin magnetic moments within 14%, 10%, and 17% and the orbital moments within 28%, 54%, and 83% for Co, Fe, and Cr, respectively (Table II). XMCD sum rules are derived within an ionic model using a number of approximations. For $L_{2,3}$, they are[27] (1) ignore the exchange splitting for the core levels, (2) replace the interaction operator $\boldsymbol{\alpha}\cdot\mathbf{a}_\lambda$ in Eq. (8) by $\boldsymbol{\nabla}\cdot\mathbf{a}_\lambda$, (3) ignore the asphericity of the core states, (4) ignore the difference of $d_{3/2}$ and $d_{5/2}$ radial wave functions, (5) ignore $p\rightarrow s$ transitions, (6) ignore the energy dependence of the radial matrix elements. To investigate the influence of the last point we applied the sum rules to the XMCD spectra calculated neglecting the energy dependence of the radial matrix elements. As can be seen from Table II using the energy independent radial matrix elements reduces the disagreement in spin magnetic moments to 4%, 2%, and 1% and in the orbital moment to 7%, 9%, and 0% for Co, Fe, and Cr, respectively. These results show that the energy dependence of the matrix elements affects strongly the values of both the spin and the

TABLE II. The experimental and calculated spin M_s and orbital M_l magnetic moments (in μ_B) of $Co_2Cr_{0.625}Fe_{0.375}Al$ (spin in orbital moments are averaged over different nonequivalent atomic positions).

Method	Atom	M_s	M_l
LSDA	Al	−0.074	0.0
	Co	0.887	0.029
	Fe	2.733	0.061
	Cr	1.524	0.006
Sum rules	Co	0.764	0.021
	Fe	2.469	0.028
	Cr	1.244	0.001
Sum rules[a]	Co	0.923	0.031
	Fe	2.787	0.056
	Cr	1.533	0.006
LSDA+U	Co	0.909	0.048
	Fe	2.700	0.083
	Cr	1.537	0.010
Expt.[b]	Co	0.96	0.12
	Fe	2.37	0.33
	Cr	0.40	0.04

[a]Sum rules applied for the XMCD spectra calculated with ignoring the energy dependence of the radial matrix elements.
[b]Reference 23.

orbital magnetic moments derived using the sum rules. The largest discrepancy was found for Cr magnetic moments, because Cr has the largest width of the *d* energy band.

The value of the orbital magnetic moments derived from the experimental XMCD spectra is considerably higher in comparison with our band structure calculations (Table II). It is a well-known fact, however, that LSDA calculations are inaccurate in describing orbital magnetism.[27,35] In the LSDA, the Kohn-Sham equation is described by a local potential which depends on the electron spin density. The orbital current, which is responsible for M_l, is, however, not included in the equations. This means, that although M_s is self-consistently determined in the LSDA, there is no framework to determine simultaneously M_l self-consistently. Numerous attempts have been made to better estimate M_l in solids. They can be roughly classified into two categories. One is based on the so-called current density functional theory[66–68] which is intended to extend density functional theory to include the orbital current as an extra degree of freedom, which describes M_l. Unfortunately an explicit form of the current density functional is at present unknown. The other category includes orbital polarization,[69–72] self-interaction correction,[73] and LSDA+U[74,75] approaches.

To calculate M_l beyond the LSDA scheme we used the rotationally invariant LSDA+U method.[75] We used $U=J=1.0$ eV for transition metal sites. In this case $U_{\text{eff}}=U-J=0$ and the effect of the LSDA+U comes from nonspherical terms which are determined by F^2 and F^4 Slater integrals. This approach is similar to the orbital polarization corrections mentioned above.[35] The LSDA+U calculations produce the orbital magnetic moments equal to $0.048\mu_B$, $0.083\mu_B$, and $0.010\mu_B$ for Co, Fe, and Cr sites, respectively. These values are somewhat larger than the LSDA values but still smaller than the experimental estimations.

The calculated total magnetic moment of $Co_2Cr_{0.6}Fe_{0.4}Al$ is $3.68\mu_B$ per unit cell. On the other hand, the total magnetic moment derived from the sum rules applied to the experimentally measured XAS and XMCD spectra was found to be only $1.34\mu_B$ per unit cell.[23] It is important to note that the sum rule derived total magnetic moment is inconsistent not only with respect to the theoretical results but most importantly also with respect to the value derived from the SQUID magnetometry measurements ($3.2\mu_B$ at 300 K and $3.5\mu_B$ extrapolated to 0 K) on the same sample.[23] This inconsistency can indicate some problems in applying the sum rules in this particular Heusler alloy. As can be seen from Table II the missing magnetic moment compared with the theoretical estimation is mainly due to a reduction of the Cr spin magnetic moment. On the other hand, the Cr L_3 and the L_2 spectra strongly overlap (see upper panel of Fig. 9). Therefore the decomposition of a corresponding experimental $L_{2,3}$ spectrum into its L_3 and L_2 parts is quite difficult and can lead to additional errors in the estimation of the magnetic moments using the sum rules [the integration $\int_{L_3}$ and $\int_{L_2}$ in Eq. (11) must be taken over the $2p_{3/2}$ and $2p_{1/2}$ absorption regions separately].

Authors of Ref. 23 suggested that in the experiment the origin of the prominent decrease of the total magnetic moment might be also a remaining disorder between Cr and Co. The calculations by Miura *et al.*[18,19] show that the antisite Cr antiferromagnetically couples with the nearest-neighbor ordinary-site Cr, and the total magnetic moment decreases with increasing the disorder. Other possibilities, such as nonstoichiometry at surface and interface may also be important in the present system.[18] For example, the observed magnetic moment of thin film $Co_2Cr_{0.6}Fe_{0.4}Al$ at 5 K is $2.04\mu_B$ per unit cell.[22] However, larger magnetic moments have been obtained for bulk $Co_2Cr_{0.6}Fe_{0.4}Al$.[15,23]

IV. SUMMARY

We have studied by means of an *ab initio* fully relativistic spin-polarized Dirac linear-muffin-tin-orbital method the electronic structure and x-ray magnetic dichroism spectra of the Heusler alloys $Co_2Cr_{1-x}Fe_xAl$ ($x=0$, 0.125, 0.25, 0.375, 0.5, 0.625, 0.75, and 1).

An important feature of the electronic structure of Co_2CrAl is a sharp peak in the DOS of the majority-spin electrons at the Fermi level. The presence of the peak at E_F can be responsible for the antisite disorder in Co_2CrAl.[18] The spin-polarized calculations show that Co_2CrAl is a half-metallic ferromagnet. The calculated total DOS shows a gap of 0.18 eV for minority spin electrons. The gap in the minority bands is due to the Co-Cr interactions as the strongest bonding interactions. The spin-orbit coupling destroys the

energy gap in the minority-spin states. Nevertheless, the spin polarization of electron states at the Fermi energy in the Heusler alloys $Co_2Cr_{1-x}Fe_xAl$ is still high (about 95%) for the compositions between $x=0$ and $x=0.4$, owing to high peaks at the Fermi energy in the majority-spin local DOS at Cr and Co atoms. Further increasing of Fe content leads to the abrupt decreasing of the spin polarization of carriers.

The local electronic and magnetic structures of Fe atoms are quite stable and depend essentially on the mean distance to other Fe atoms. The concentration and arrangement of Fe atoms in the lattice play the leading role in the formation of the magnetic properties of the compounds, determining to a considerable extent the magnetic states of Co and Cr atoms. In these circumstances the properties of doped compounds may be sensitive to the techniques of the sample preparation or to the kind of heat treating, whether Fe atoms are statistically distributed over the whole lattice or they create Fe-rich clusters in the doped compound.

The band structure calculations in the LSDA approximation reproduce quite well the shape of the XAS and XMCD spectra at the Co, Fe, and Cr $L_{2,3}$ edges. The magnetic dichroism at the $M_{2,3}$ edge is much smaller than at the $L_{2,3}$ edge. Besides the M_2 and the M_3 spectra are strongly overlapped due to the small spin-orbit splitting of the $3p$ core levels. The exchange splitting of the initial $1s$-core state is extremely small therefore only the exchange and spin-orbit splitting of the final $4p$ states is responsible for the observed dichroism at the K edge. For this reason the dichroism is found to be very small (three orders of magnitude less intensive in comparison with the dichroism at the $L_{2,3}$ edges). The energy dependence of the matrix elements affects strongly the values of both the spin and the orbital magnetic moments derived from the calculated XAS and XMCD spectra using the sum rules.

Our calculations show that the magneto-optical measurements are sensitive to changes in the structure of compounds (doping, disorder, etc.) accompanied by changes of the magnetic states of atoms. To our knowledge, the last systematical magneto-optical investigations[49,50] of Heusler alloys were performed over 20 years ago, and recent accurate magneto-optical results (especially for doped compounds) are still lacking. These measurements however seem to be very useful.

ACKNOWLEDGMENTS

This work was supported by the Deutsche Forschungsgemeinschaft (DFG) under Grant No. 436 UKR 17/12/03 as well as the CRDF Contract No. 14589.

[1] F. Heusler, Verh. Dtsch. Phys. Ges. **5**, 219 (1903).
[2] P. J. Webster and K. R. A. Ziebeck, in *Alloys and Compounds of d-Elements with Main Group Elements*, edited by H. R. J. Wijn (Springer-Verlag, Berlin, 1988), Vol. 19/C of Landolt-Börnstein, New Series, Group III, pp. 75–184.
[3] K. R. A. Ziebeck and K.-U. Neumann, in *Magnetic Properties of Metals*, edited by H. R. J. Wijn (Springer-Verlag, Berlin, 2001), Vol. 32/C of Landolt-Börnstein, New Series, Group III, pp. 64–414.
[4] G. A. Prinz, Science **282**, 1660 (1998).
[5] R. A. de Groot, F. M. Mueller, P. G. van Engen, and K. H. J. Buschow, Phys. Rev. Lett. **50**, 2024 (1983).
[6] C. Felser *et al.*, J. Phys.: Condens. Matter **15**, 7019 (2003).
[7] I. Galanakis, J. Phys.: Condens. Matter **14**, 6329 (2002).
[8] K. Nagao, M. Shirai, and Y. Miura, J. Phys.: Condens. Matter **16**, S5725 (2004).
[9] I. Galanakis, J. Phys.: Condens. Matter **16**, 8007 (2004).
[10] K. R. A. Ziebeck and P. J. Webster, J. Phys. Chem. Solids **35**, 1 (1974).
[11] A. Jezierski, Phys. Status Solidi B **196**, 357 (1996).
[12] M. Pugaczowa-Michalska, J. Magn. Magn. Mater. **185**, 35 (1998).
[13] K. Kaczmarska, J. Pierre, J. Tobola, and R. V. Skolozdra, Phys. Rev. B **60**, 373 (1999).
[14] A. Ślebarski, M. B. Maple, A. Wrona, and A. Winiarska, Phys. Rev. B **63**, 214416 (2001).
[15] T. Block, C. Felser, G. Jakob, J. Ensling, B. Mühling, P. Gütlich, and R. J. Cava, J. Solid State Chem. **176**, 646 (2003).
[16] I. Galanakis, P. H. Dederichs, and N. Papanikolaou, Phys. Rev. B **66**, 174429 (2002).
[17] I. Galanakis, J. Phys.: Condens. Matter **16**, 3089 (2004).
[18] Y. Miura, K. Nagao, and M. Shirai, Phys. Rev. B **69**, 144413 (2004).
[19] Y. Miura, M. Shirai, and K. Nagao, J. Appl. Phys. **95**, 7225 (2004).
[20] T. Block, M. J. Carey, B. A. Gurney, and O. Jepsen, Phys. Rev. B **70**, 205114 (2004).
[21] I. Galanakis, Phys. Rev. B **71**, 012413 (2005).
[22] K. Inomata, S. Okamura, R. Goto, and N. Tezuka, Jpn. J. Appl. Phys., Part 2 **42**, L419 (2003).
[23] H. J. Elmers *et al.*, Phys. Rev. B **67**, 104412 (2003).
[24] H. Kubota, J. Nakata, M. Oogane, Y. Ando, A. Sakuma, and T. Miyazaki, Jpn. J. Appl. Phys., Part 2 **43**, L984 (2004).
[25] K. Kobayashi, R. Y. Umetsu, R. Kainuma, K. Ishida, T. Oyamada, A. Fujita, and K. Fukamichi, Appl. Phys. Lett. **85**, 4684 (2004).
[26] R. Y. Umetsu, K. Kobayashi, R. Kainuma, A. Fujita, K. Fukamichi, K. Ishidaa, and A. Sakuma, J. Appl. Phys. **85**, 2011 (2004).
[27] H. Ebert, Rep. Prog. Phys. **59**, 1665 (1996).
[28] J. P. Hannon, G. T. Trammell, M. Blume, and D. Gibbs, Phys. Rev. Lett. **61**, 1245 (1988).
[29] S. W. Lovsey and S. P. Collins, *X-Ray Scattering and Absorption in Magnetic Materials* (Oxford University Press, Oxford, 1996).
[30] J. B. Kortright and S.-K. Kim, Phys. Rev. B **62**, 12216 (2000).
[31] W. H. Kleiner, Phys. Rev. **142**, 318 (1966).
[32] W. Reim and J. Schoenes, in *Ferromagnetic Materials*, edited by E. P. Wohlfarth and K. H. J. Buschow (North-Holland, Amsterdam, 1990), Vol. 5, p. 133.
[33] R. Kubo, J. Phys. Soc. Jpn. **12**, 570 (1957).
[34] C. S. Wang and J. Callaway, Phys. Rev. B **9**, 4897 (1974).
[35] V. Antonov, B. Harmon, and A. Yaresko, *Electronic Structure and*

Magneto-Optical Properties of Solids (Kluwer Academic, Dordrecht, 2004).
[36] A. Santoni and F. J. Himpsel, Phys. Rev. B **43**, 1305 (1991).
[37] F. K. Richtmyer, S. W. Barnes, and E. Ramberg, Phys. Rev. **46**, 843 (1934).
[38] B. T. Thole and G. van der Laan, Phys. Rev. B **38**, 3158 (1988).
[39] B. T. Thole, P. Carra, F. Sette, and G. van der Laan, Phys. Rev. Lett. **68**, 1943 (1992).
[40] P. Carra, B. T. Thole, M. Altarelli, and X. Wang, Phys. Rev. Lett. **70**, 694 (1993).
[41] G. van der Laan and B. T. Thole, Phys. Rev. B **53**, 14458 (1996).
[42] V. N. Antonov, B. N. Harmon, and A. N. Yaresko, Phys. Rev. B **63**, 205112 (2001).
[43] V. N. Antonov, B. N. Harmon, and A. N. Yaresko, Phys. Rev. B **66**, 165208 (2002).
[44] V. N. Antonov, B. N. Harmon, and A. N. Yaresko, Phys. Rev. B **66**, 165209 (2002).
[45] O. K. Andersen, Phys. Rev. B **12**, 3060 (1975).
[46] V. V. Nemoshkalenko, A. E. Krasovskii, V. N. Antonov, V. N. Antonov, U. Fleck, H. Wonn, and P. Ziesche, Phys. Status Solidi B **120**, 283 (1983).
[47] J. P. Perdew and Y. Wang, Phys. Rev. B **45**, 13244 (1992).
[48] P. E. Blöchl, O. Jepsen, and O. K. Andersen, Phys. Rev. B **49**, 16223 (1994).
[49] K. H. J. Buschow and P. G. van Engen, J. Magn. Magn. Mater. **25**, 90 (1981).
[50] K. H. J. Buschow, P. G. van Engen, and R. Jongebreur, J. Magn. Magn. Mater. **38**, 1 (1983).
[51] K. H. J. Buschow, in *Ferromagnetic Materials*, edited by E. P. Wohlfarth and K. H. J. Buschow (North-Hollandx, Amsterdam, 1988), Vol. 4, p. 588.
[52] P. Villars and L. D. Calvert, *Pearson's Handbook of Crystallographic Data for Intermetallic Phases* (ASM International, Materials Park, OH, 1991).
[53] M. Zhang, Z. Liu, H. Hu, G. Liu, Y. Cui, J. Chen, G. Wu, X. Zhang, and G. Xiao, J. Magn. Magn. Mater. **277**, 130 (2004).
[54] J. C. Fuggle and J. E. Inglesfield, *Unoccupied Electronic States. Topics in Applied Physics* (Springer, New York, 1992), Vol. 69.
[55] P. Mavropoulos1, I. Galanakis, V. Popescu, and P. H. Dederichs, J. Phys.: Condens. Matter **16**, S5759 (2004).
[56] P. Mavropoulos, K. Sato, R. Zeller, P. H. Dederichs, V. Popescu, and H. Ebert, Phys. Rev. B **69**, 054424 (2004).
[57] S. Uba, L. Uba, A. Y. Perlov, A. N. Yaresko, V. N. Antonov, and R. Gontarz, J. Phys.: Condens. Matter **9**, 447 (1997).
[58] L. Uba, S. Uba, V. N. Antonov, A. N. Yaresko, and R. Gontarz, Phys. Rev. B **64**, 125105 (2001).
[59] A. Yamasaki, S. Imada, R. Arai, H. Utsunomiya, S. Suga, T. Muro, Y. Saitoh, T. Kanomata, and S. Ishida, Phys. Rev. B **65**, 104410 (2002).
[60] J. Schwitalla and H. Ebert, Phys. Rev. Lett. **80**, 4586 (1998).
[61] H. Ebert, J. Phys.: Condens. Matter **1**, 9111 (1989).
[62] G. G. Scott, J. Phys. Soc. Jpn. **17**, 372 (1962).
[63] W. Marshall and S. W. Lovsey, *Theory of Thermal Neutron Scattering* (Oxford University Press, Oxford, 1971).
[64] M. Blume, J. Appl. Phys. **57**, 3615 (1985).
[65] I. Galanakis, S. Ostanin, M. Alouani, H. Dreyssé, and J. M. Wills, Phys. Rev. B **61**, 4093 (2000).
[66] G. Vignale and M. Rasolt, Phys. Rev. Lett. **59**, 2360 (1987).
[67] P. Skudlarski and G. Vignale, Phys. Rev. B **48**, 8547 (1993).
[68] M. Higuchi and A. Hasegawa, J. Phys. Soc. Jpn. **66**, 149 (1997).
[69] M. S. S. Brooks, Physica B & C **130B**, 6 (1985).
[70] O. Eriksson, M. S. S. Brooks, and B. Johansson, Phys. Rev. B **41**, R7311 (1990).
[71] L. Severin, M. S. S. Brooks, and B. Johansson, Phys. Rev. Lett. **71**, 3214 (1993).
[72] A. Mavromaras, L. Sandratskii, and J. Kübler, Solid State Commun. **106**, 115 (1998).
[73] S. V. Beiden, W. M.Temmermann, Z. Szotek, and G. A. Gehring, Phys. Rev. Lett. **79**, 3970 (1997).
[74] I. V. Solovyev, A. I. Liechtenstein, and K. Terakura, Phys. Rev. Lett. **80**, 5758 (1998).
[75] A. N. Yaresko, V. N. Antonov, and P. Fulde, Phys. Rev. B **67**, 155103 (2003).